

Topography of Cones and Rods in the Tree Shrew Retina

BRIGITTE MÜLLER AND LEO PEICHL

Max-Planck-Institut für Hirnforschung, D-6000 Frankfurt/Main 71,
Federal Republic of Germany

ABSTRACT

The topographical distribution of cones and rods in the tree shrew retina was analysed quantitatively in whole-mounted retinae and horizontal semi-thin sections stained with cresyl violet or toluidine blue. The outer nuclear layer consists of a single layer of photoreceptor nuclei with the rod nuclei slightly displaced towards the outer plexiform layer. This facilitated quantification of the photoreceptor populations. The density of cones ranges from $12,000/\text{mm}^2$ in the peripheral retina to a maximum of $36,000/\text{mm}^2$ in the inferior retina. Unlike ganglion cell density, the density of cones does not peak in the temporal retina. Rod density, between $500/\text{mm}^2$ and $3,500/\text{mm}^2$, also peaks in the inferior retina, but not in the same region as cone density. Rods constitute from 1 to 14% of the photoreceptor population, depending on retinal location, and have a local minimum at the central area. Amongst the cones a regularly arrayed subpopulation of presumed blue-sensitive cones is distinguished by its special staining properties. These cones constitute between 4 and 10% of the cone population depending on retinal location. A second, irregularly spaced, subpopulation of possibly pathological cones is also described.

Key words: photoreceptor distribution, blue cones, *Tupaia*

Tree shrews (*Tupaia belangeri*) are diurnal omnivores living in an arboreal habitat in the forest areas of southeastern Asia. They have a well-developed visual system. Their retinae are cone-dominated, in contrast to the common mammalian pattern of rod-dominated retinae. Early light microscopic studies even described the tree shrew as having a pure cone retina (Castenholz, '65; Rohen and Castenholz, '67). Polyak ('57), however, mentioned a rod population, and electron microscopy revealed photoreceptors with rodlike features (Samorajski et al., '66; Dieterich, '69; Kühne, '83). Recent studies estimate that the rod population composes about 4% of photoreceptors (Immel and Fisher, '85; Foelix et al., '87). The cone-dominated tree shrew retina with its relatively small rod population is an example of a distinct phylogenetic specialization, comparable to the foveal region of primate retina (Samorajski et al., '66). The present paper establishes the distributions and proportions of the photoreceptor types. We describe the presence of presumed blue-sensitive cones and analyse the topography of this subpopulation, of all cones, and of the rods.

The tree shrew has laterally positioned eyes and hence a wide panoramic view, but there is still a binocular field of some $50-60^\circ$ (Polyak, '57). In temporal retina the blood vessel pattern and the ganglion cell distribution mark a central area in a rather peripheral position, within the binocular

field representation (DeBruyn, '83; present results). It turned out that both cones and rods have their highest densities in the inferior retina, not at the central area. Thus the tree shrew proves not only to be exceptional in its cone dominance but also in the way the photoreceptors are mapped onto the ganglion cells.

MATERIALS AND METHODS

Thirteen adult tree shrews (*T. belangeri*), both male and female, were used for the present study. Most of the animals were obtained from breeding colonies (at our institute, and at the German Primate Centre, Göttingen), some were specimens captured from the wild in Malaysia (caught by Prof. D. Pye; the eyes were made available to us through Prof. B.B. Boycott). The animals were overdosed with pentobarbital, given intraperitoneally, and the eyes were enucleated directly postmortem. Before enucleation, orientation of the eyes was marked by a thread through the sclera at the superior pole of the eye. The eyeball was cut open around

Accepted December 13, 1988.

Address reprint requests to Brigitte Müller, MPI für Hirnforschung, Neuroanatomische Abteilung, Deutscher Straße 46, D-6000 Frankfurt/M. 71, Federal Republic of Germany.

the equator, the anterior part with lens and vitreous was removed, and the posterior eyecup with the retina attached was immersed in the fixative (4 or 2% formalin in physiological saline or phosphate buffer (PB 0.1 M, pH 7.4)). After at least 1.5 hours in the fixative the orientation was marked by a cut in superior retina, and the retina was removed from the eyecup. Total fixation time varied between 2 hours and a few months; the eyes of the wild tree shrews were in the fixative for 5 years. Any pigment epithelium still adhering to the retina was carefully brushed off and four to six radial cuts were made to flatten the retina.

Histological procedures

Some retinae were embedded flat and sectioned horizontally. After fixation these retinae were dehydrated in ethanol between a sandwich of filter papers on a glass slide and embedded flat in glycol methacrylate (LKB 2218-500 HISTORESIN Embedding Kit). The procedure is a modification of that described by Polley and Walsh ('84). Flat sections 5 µm thick were taken on a microtome (Jung, Ultracut 1150) by using a glass knife (38 mm wide). Sections obtained in this way contained the whole retinal area or at least large parts of it and thus simplified the topographical analysis. Series of sections were mounted on glass slides and stained with 0.05% toluidine blue for a few seconds. After drying on a warm plate (60°C) they were mounted in Permount (Fisher) and coverslipped.

Other retinae were analysed as whole-mounts. These were mounted vitreal-side or photoreceptor-side up onto gelatinized slides and stained with cresyl violet following the protocol of Wässle et al. ('75).

To reveal the presumed blue-sensitive cone subpopulation a photoreceptor-specific polyclonal antibody against bovine S-antigen ("SAP") was used for immunocytochemical staining of retinal semithin sections (embedded in paraffin) and whole isolated retinae. (For details of the protocol see Korf et al., '85; Müller et al., '89).

Microglial cells of the outer plexiform layer have their nuclei at the level of the rod nuclei and are thus a possible source of error. To assess their density, microglial cells were identified histochemically in one retina by demonstrating thiamine pyrophosphatase (TTPase) activity by using the method of Novikoff and Goldfischer ('61) and manganese chloride as the activator. The retina was immersion fixed in 4% paraformaldehyde, 8% sucrose, and 5% dimethylsulfoxide in 0.1 M cacodylate buffer (pH 7.2) for 4 hours at 4°C and stained according to the protocol of Terubayashi et al. ('84). Cells were analysed in whole-mounts and in vibratome sections.

The blood vessels of the ganglion cell layer proved to be a reliable intraretinal landmark system. To visualise the detailed pattern of this blood vessel system, retinae were treated with diamino benzidine (DAB) solution. In the presence of DAB the endogenous peroxidase of red blood cells reacts to form a visible product; the endothelial cells of the blood vessel walls are also visualized by the method. After fixation for 1.5 hours the retina was rinsed in several changes of 0.1 M phosphate buffer for 1.5 hours. After incubation in a 0.05% DAB solution (Sigma) for 10 minutes, the retina was transferred to a 0.05% DAB solution containing 0.02% hydrogen peroxide for 15 minutes. After several washes the whole retina was mounted on a gelatinized slide, vitreal-side up, dehydrated, cleared, mounted in Permount, and coverslipped.

Evaluation of populations

Maps of whole-mounted retinae were drawn with a low-power objective ($\times 1.25$ or $\times 2.5$) and a Zeiss drawing tube. The superior radial cut, the retinal blood-vessel pattern, and the position of the optic disc were used to orient the retinae and mark the positions of areas to be analysed. The densely packed cone population was drawn with a $\times 100/1.3$ oil-immersion objective (Zeiss Neofluar; sample field size $100 \times 100 \mu\text{m}$). The more sparsely distributed rod population was drawn with a $\times 40/1.0$ oil-immersion objective (Zeiss Planapo; sample field size $250 \times 250 \mu\text{m}$). One hundred sixty to 320 sample fields per retina were analysed for the density maps in Figures 5 and 6, as were 70–130 sample fields for the maps in Figures 8 and 12. Drawings of horizontal sections were obtained in the same way and the map of the entire retina was reconstructed from these drawings. Shrinkage was assessed by comparing retinal size before histological treatment with that after mounting and was 3–10% in area. The maps of photoreceptor densities are not corrected for shrinkage. The mosaics of rods and the presumed blue-sensitive cone subpopulation were examined by a nearest-neighbour analysis (Wässle and Riemann, '78). The total numbers of rods and cones per retina were estimated by integration of the isodensity lines in the maps of Figure 5.

The terms *temporal*, *nasal*, *superior*, *inferior*, and *central* are used here with respect to the optic disc, not with respect to the central area, which hence is located in temporal retina.

Abbreviations

PE	pigment epithelium
PR	photoreceptor layer
IS	inner segments
ONL	outer nuclear layer
OPL	outer plexiform layer
INL	inner nuclear layer
IPL	inner plexiform layer
GCL	ganglion cell layer
r	rod nucleus
m	microglial nucleus
bc	blue cone nucleus
dc	dark cone nucleus
TTPase	thiamine pyrophosphatase

Fig. 1. Toluidine-blue-stained vertical and horizontal semithin sections through the tree shrew retina. A: Vertical section of midperipheral retina showing the proportions of the retinal layers. B: Outer retina with photoreceptors, outer plexiform layer, and a part of the inner nuclear layer at higher power. Photoreceptor nuclei are arranged in a single layer; the rod nuclei (r) appear darker than the cone nuclei and are slightly displaced toward the OPL. The nucleus of a microglial cell (m) is found at the same level. It has no cytoplasmic extrusion into the stratum of receptor inner segments. C–F: Horizontal sections through the photoreceptor layer at four different planes. C: Level of cone inner and rod outer segments. The latter (one arrowed) are barely recognisable between the large cone profiles. A regularly spaced subpopulation of cone inner segments is more darkly stained. D: Cones (large light profiles) and rods (thin arrows) at the level of the outer limiting membrane. The blue cone population (darker profiles) and two dark cones (arrowheads) are apparent. E: Level of the outer nuclear layer, showing the cone nuclei and some barely visible rod inner segments (thin arrows). Some cone nuclei are darker and more polygonal than the other cone nuclei (arrowheads). F: Level of rod nuclei at the boundary between ONL and OPL. The unstained profiles are cone pedicles. All scale bars are 20 µm, the scale bar in C–F applies to C–F.

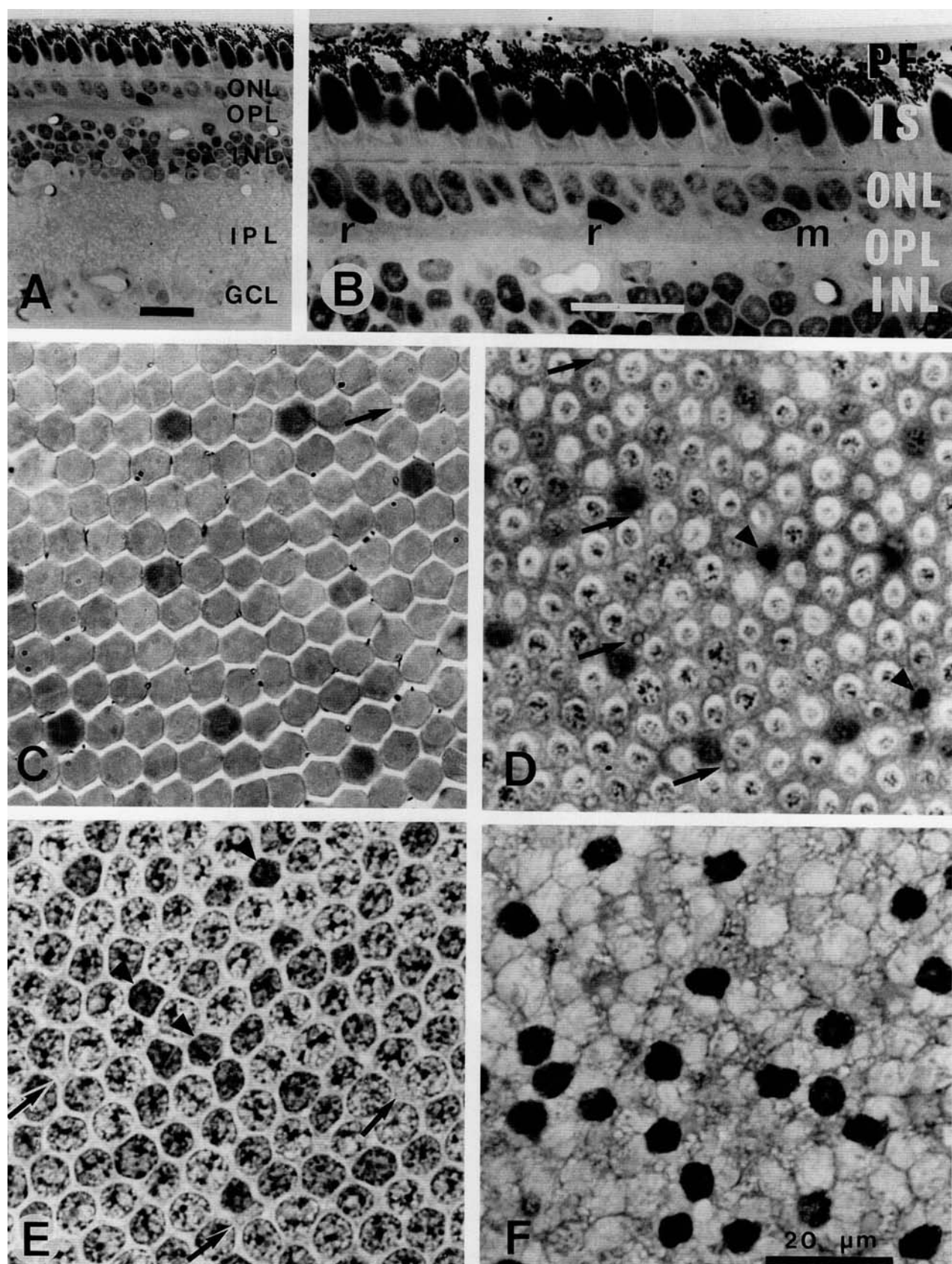


Figure 1

RESULTS

Identification of rods and cones

In contrast to most mammalian retinae, the tree shrew retina has an outer nuclear layer (ONL) that consists of a single row of photoreceptor somata (Fig. 1A,B). This organization facilitates quantitative analysis of both cones and rods. As shown by Foelix et al. ('87), rods and cones can be distinguished in vertical sections by the differing positions of their cell compartments. Figure 1B shows a vertical section through the outer retina with photoreceptors, outer plexiform layer (OPL), and part of the inner nuclear layer (INL). The cone nuclei form a tight layer and are lightly stained whereas the rod nuclei are darkly stained and are somewhat displaced toward the OPL.

Horizontal sections through the photoreceptor layer at four different planes of section are depicted in Figure 1C–F. At the level of the cone inner and rod outer segments (C) the latter (one arrowed) are barely recognizable between the large cone profiles. Rods (arrows) and cones (large light profiles) can be seen at the level of the outer limiting membrane (D). In E the plane of section runs through the ONL cutting all cone nuclei, some of which are more polygonal and darker than the others (arrowheads). The very faintly stained rod inner segments in between the well-stained cone nuclei are barely visible in this micrograph (arrows). Finally, the darkly stained rod nuclei can be seen when the plane of section runs through the junction of the ONL/OPL (F).

Sections through the retina at the border of the ONL/OPL were most appropriate for quantification of the rod population. The cone population was quantified in horizontal sections through the cone inner segments (C) or through their nuclei (E). Alternatively, whole mounts were used.

Amongst the cones a regularly arrayed subpopulation stains more intensely. This is very prominent at the level of the inner segments, Figure 1C, but also apparent in Figure 1D,E. In addition a second, more randomly spaced, cone subpopulation with polygonal, darkly stained profiles is recognizable in horizontal sections (Fig. 1D,E: arrowheads). These two subpopulations were also seen by Foelix et al. ('87) in vertical sections.

Microglial cells

In addition to the rod nuclei, another type of nucleus was observed at the proximal level of the outer nuclear layer (Müller et al., '89). These nuclei differed from the rod nuclei in their shape and stained appearance, often being smaller and sometimes triangular. They had numerous evenly distributed chromatin granules and thus often appeared smoother and more translucent with the nuclear membrane easily distinguishable. One of these nuclei appears in Figure 1B (m). The presence of microglia in the OPL of other mammals (Boycott and Hopkins, '81; Dräger, '83) suggested that these nuclei might also be microglial. Application of a microglia-specific histochemical method (Novikoff and Goldfischer, '61; Terubayashi et al., '84) produced direct evidence that the nuclei belonged to microglial cells. This microglial population is evenly distributed across the retina at a uniform density of about 100 cells/mm². The processes of the microglial cells do not overlap but cover the retina without large gaps (Fig. 2). When determining rod densities, microglial nuclei were not counted.

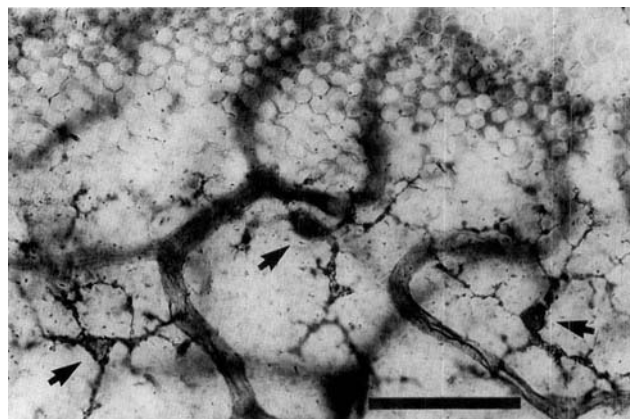


Fig. 2. Microglial cells in the outer plexiform layer. Three microglial cells are visible in this nearly horizontal 50 µm vibratome section through the OPL/ONL border (arrows). The top of the section contains some cone nuclei, and at the bottom the OPL capillary bed is marked by thiamine pyrophosphatase (TPPase) activity. Scale bar equals 50 µm.

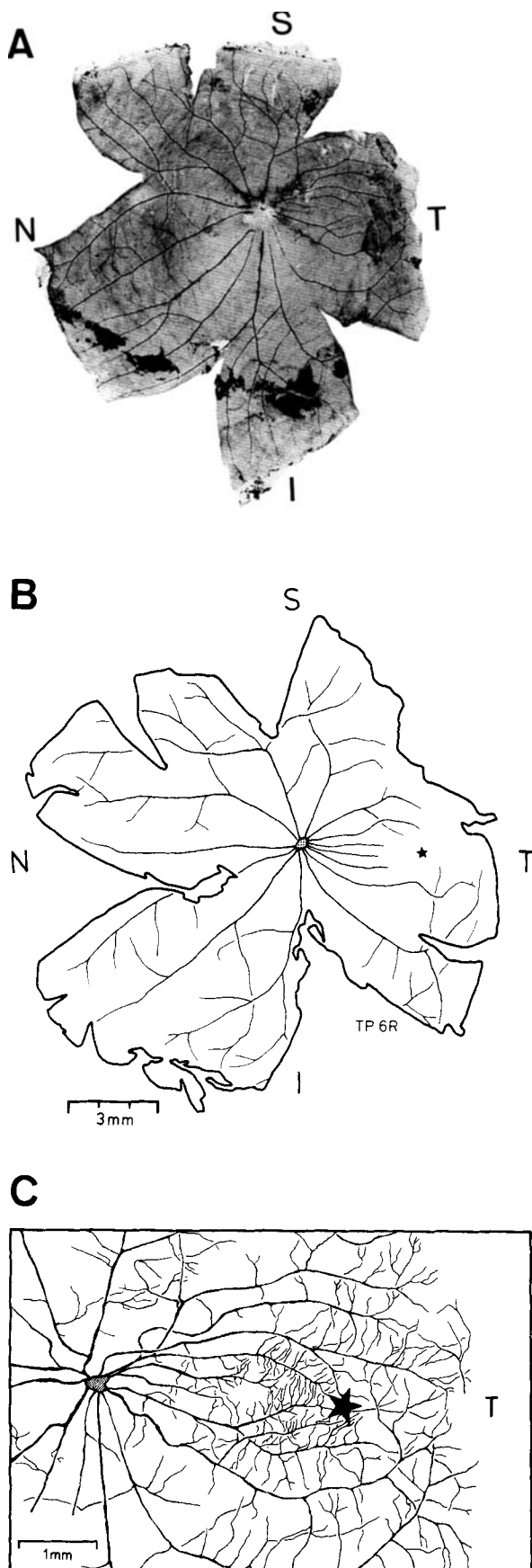
The pattern of blood vessels in the ganglion cell layer: A retinal landmark system

For topographical analysis of photoreceptor distributions a reliable intraretinal landmark system was sought. The retinal blood-vessel system in the ganglion cell layer (GCL) has consistent asymmetries that are pronounced enough to allow unequivocal orientation of the retina. The retinal blood vessels can best be seen when DAB treated, but they are also traceable in Nissl-stained preparations.

Figure 3A shows a whole-mounted retina, ganglion cell layer uppermost, with the blood vessels visualized by the peroxidase reaction. The optic disc is not localized at the geometric centre of the retina; distances to the temporal and superior retinal margins (ora serrata) are shorter than those to the nasal and inferior margins. The primary blood vessels radiate from the optic disc, except in the temporal retina, where they form pincers in a region of about 1.5 mm². This appears very similar to the blood-vessel arrangement around the central area of the cat retina, or the fovea of primates, which itself is free of blood vessels. In tree shrew, too, the centre of this blood-vessel specialization is the region of highest ganglion cell density (DeBruyn, '83; Müller and Peichl, unpublished observations). In the tree shrew this central area lies about 1.5 mm away from the temporal ora serrata, and is therefore much more peripheral than in primates and cats. The blood vessel pattern in temporal retina, drawn in Figure 3C at higher magnification, was common to all 13 animals. The total number of primary blood vessels varied, however. One animal had ten, one 14 (Fig. 3B) and all others 18 primary blood vessels (Fig. 3A), and the numbers were the same for both retinae in each animal. In conclusion, the GCL blood-vessel pattern in temporal retina could be used to orient the retinae and recognize the position of the central area.

Topographical distributions of photoreceptors

Figure 4 illustrates the range of densities found in the cone and rod populations. Cone diameters decrease with



increasing cone density; because cones are densely packed density and diameter are inversely related. The smallest cone nuclear diameters are $3 \mu\text{m}$, the largest $8 \mu\text{m}$. By contrast, the sizes of rod nuclei remain unaffected by density changes. They have a mean diameter of $5\text{--}6 \mu\text{m}$ and are often oval. The regularity of spacing in the cone mosaic is a consequence of the dense packing that approaches hexagonal symmetry (Figs. 1C, 4A,B). The rod nuclei are more randomly arrayed (Fig. 4C,D).

Cones. Maps of the cone density distribution in three retinae are presented in Figure 5A-C. Cone densities are given as isodensity lines which encircle areas of higher density. The cone isodensity lines are horizontally elongated. Toward inferonasal retina the density gradient becomes steeper. The lowest cone density of $12,000/\text{mm}^2$ is found in superior far periphery and the highest density of $32,000/\text{mm}^2$ in inferonasal periphery ($36,000/\text{mm}^2$ in one case) at two separate plateaus. Generally the density decreases toward far peripheral retina with the steepest gradients observed in lower retina. Cone density changes by a factor of three between the minimum in superior far periphery and the maximum in inferonasal midperiphery. An unexpected finding is that there exists no local cone density maximum in temporal retina at the location of the central area. The exact position of the cone density maxima varies somewhat between retinae (see Discussion).

The density maps of Figure 5 are not corrected for shrinkage. The different shrinkage factors (see figure legend) account for only a part of the density differences observed between the three retinae. These differences might therefore represent interindividual variability.

Rods. Rod density maps for the same three retinae are given in Figure 5D-F. In inferior far periphery the density of rods is maximal ($3,000\text{--}3,500/\text{mm}^2$). Density decreases toward the upper retina, until the lowest density of about 200 rods/mm^2 is reached in superior and temporal periphery. The decrease in rod density is most noticeable in temporal retina. Even a local minimum was found in the temporal quadrant of one retina (Fig. 5E). In all retinae studied, the rod density in temporal retina was below $500/\text{mm}^2$. The rod density ratio between temporal retina and the maximum in inferior periphery is about 1:15.

In summary, the cone and rod distributions show the following features: 1) the density maxima of cones and rods are both in inferior retina but at different locations, with the rod maximum more peripherally; 2) cone density shows no local maximum in temporal retina, i.e., no specialization associated with the central area; 3) rod density has a minimum in temporal retina; 4) density changes across the retina are much higher for rods (15:1) than for cones (3:1); and 5) maximal cone densities (about $32,000/\text{mm}^2$) are ten times higher than maximal rod densities (about $3,000/\text{mm}^2$).

Absolute numbers of photoreceptors per retina were estimated from the maps of Figure 5. In the three retinae cone

Fig. 3. Pattern of major blood vessels in the ganglion cell layer of the tree shrew retina. A: Photograph of a whole-mounted left retina treated with diaminobenzidine (DAB); 18 primary blood vessels are visible. B: Drawing of a right retina with 14 primary blood vessels, reconstructed from consecutive semithin horizontal sections. The drawing is reversed for better comparison with the left retina (A,C). C: Higher-power drawing of the temporal quadrant of the retina in A to show the blood-vessel arrangement in more detail. The blood vessels are thinner than elsewhere and embrace a region of 1.5 mm^2 centered on the central area (star). For details see text. Scale bar in B applies to A and C.

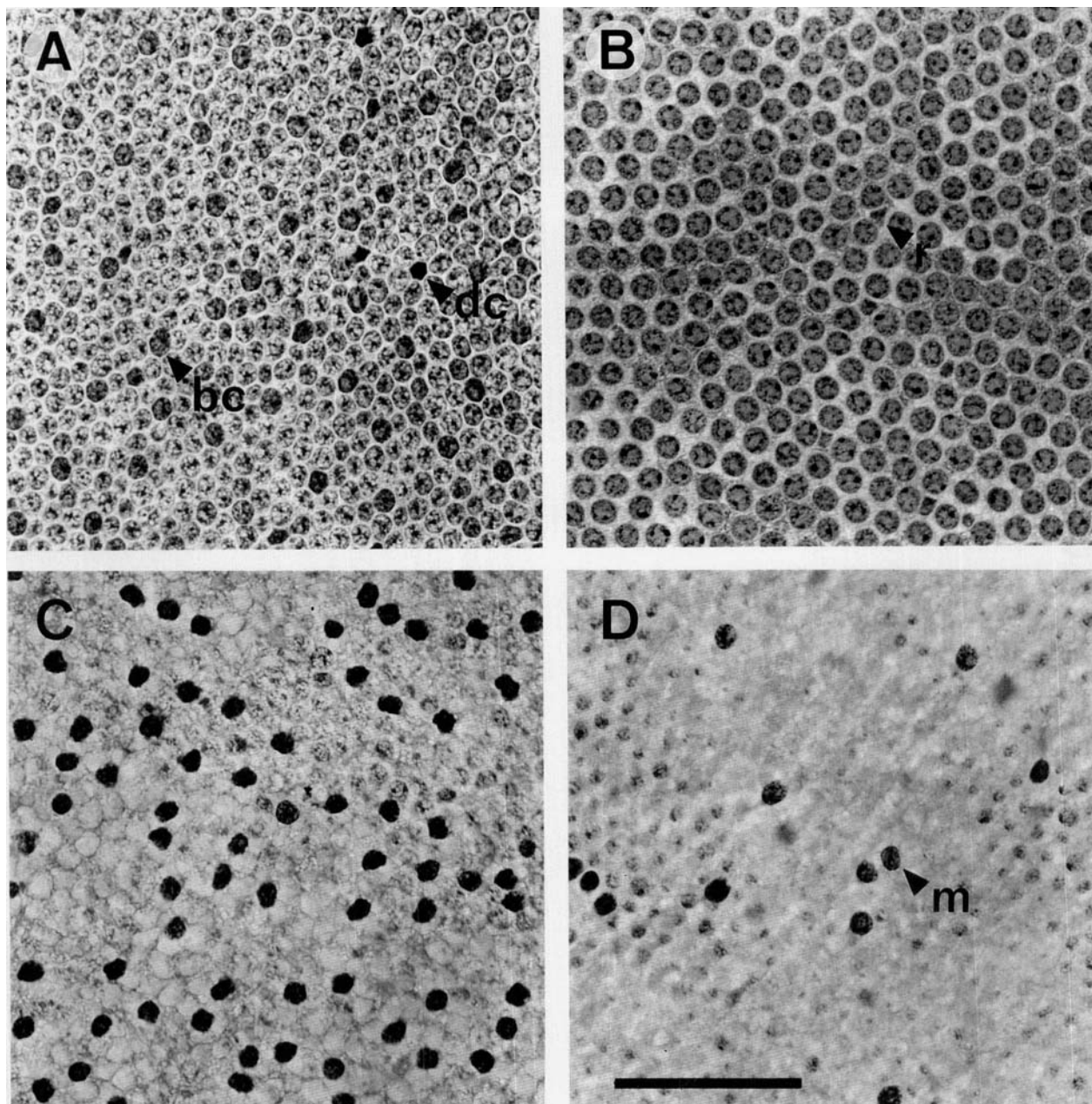


Fig. 4. Changes of photoreceptor densities across the retina. Horizontal sections through the cone nuclei (A,B) and rod nuclei (C,D), stained with toluidine blue. A: Region in nasal retina with a high cone density of about $30,000/\text{mm}^2$. The regularly arrayed cone subpopulation with somewhat larger, darker-stained nuclei is the presumed blue-sensitive cone population (bc). The few very dark polygonal profiles are the dark cones (dc). B: Region in superior retina with a cone density mini-

mum, about $13,000/\text{mm}^2$. The cone nuclear diameter increases with decreasing density. One rod inner segment (r) is marked. C: Region of high rod density in inferior retina containing about $3,500 \text{ rods/mm}^2$. D: Region of low rod density, about 500 rods/mm^2 , in superior retina. There is one microglial nucleus (m) amongst the rod nuclei. Scale bar in D equals $50 \mu\text{m}$ for A-D.

Fig. 5. Maps of photoreceptor densities in retinae from three animals. The maps show isodensity lines which encircle areas of higher densities. The stippled area in each retina represents the papilla; the star in temporal retina marks the position of the central area. Density values are given in thousands per mm^2 and not corrected for shrinkage. A-C: Cone density maps; highest cone densities occur in inferior retina forming two plateaus with steep lateral gradients in each retina. Lowest den-

sities are found in superior far periphery. D-F: Rod density maps for the same retinae; highest rod densities occur in inferior far periphery, also forming a plateau with steep slopes toward the inferior edge. Rod density decreases toward superior periphery and especially toward temporal retina (central area). In E there is even a local minimum in the temporal quadrant. Areal shrinkage of the retina was 3% in TP6R, 5% in TP5L, and 10% in TP10L. The star marks the position of the central area.

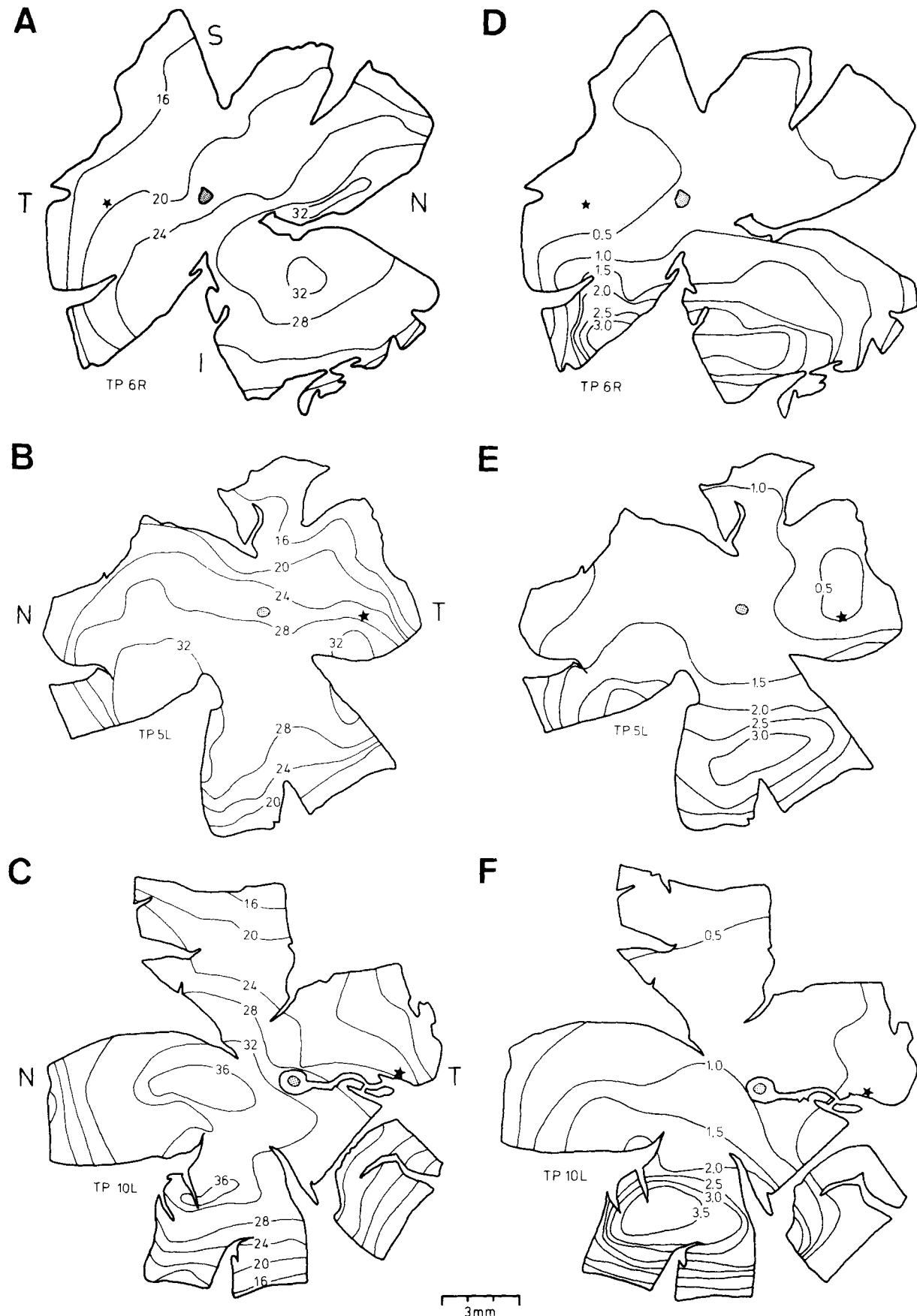


Figure 5

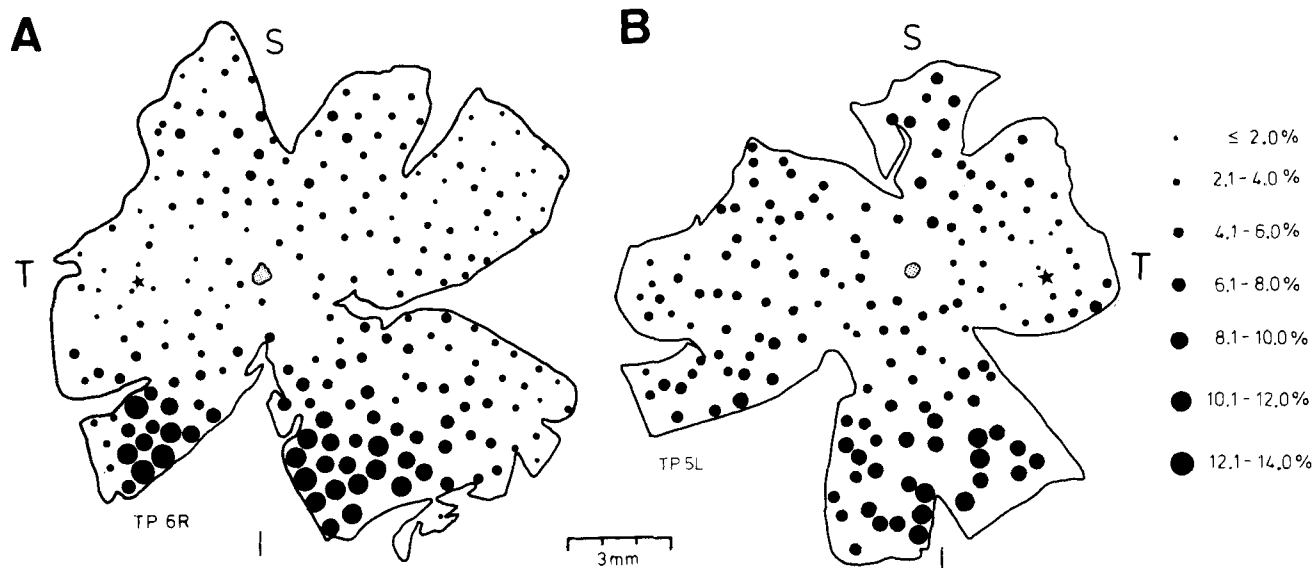


Fig. 6. Maps of the proportion of rods in the photoreceptor population of two retinas. Each dot marks a sample field and its diameter represents the local rod percentage in that field. Highest percentages are localized in inferior retina. The minimum rod percentage is near the cen-

tral area in temporal retina. Shrinkage, which affects retinal distances but not percentage values, is not corrected for. The star marks the position of the central area.

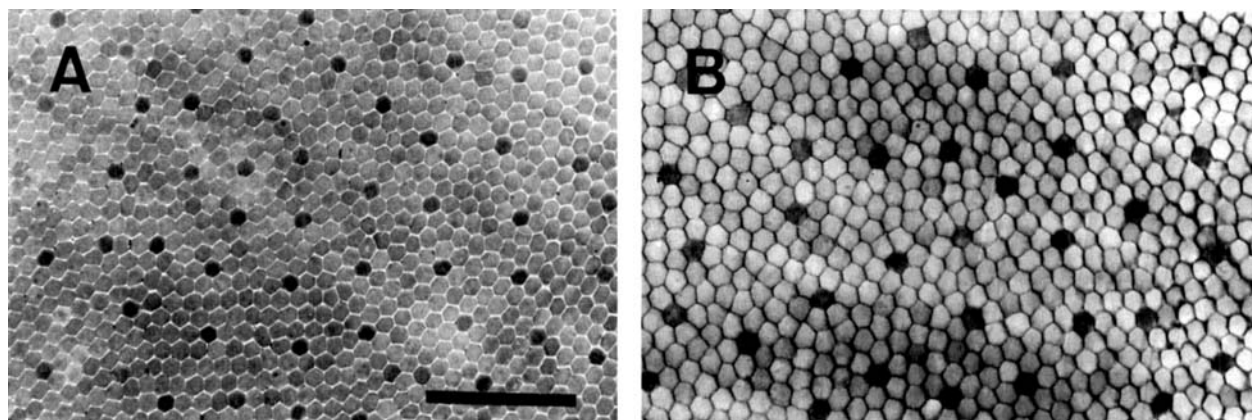


Fig. 7. Regular distribution of the intensely stained subpopulation of presumed blue-sensitive cones at two retinal locations. Micrographs of horizontal semithin sections, stained with toluidine blue. **A:** Region in inferior retina containing $28,500 \text{ cones}/\text{mm}^2$ of which $1,800/\text{mm}^2$ (6.3%)

are presumed blue cones. **B:** Region of low cone density in superior periphery with $17,500 \text{ cones}/\text{mm}^2$ of which $1,100/\text{mm}^2$ (6.3%) are presumed blue cones. Scale bar in A equals $50 \mu\text{m}$ for A and B.

numbers range from 3 to 4 million and rod numbers range from 145 to 180 thousand. Maximal cone and rod numbers are not found in the same retina; the global rod percentage is 4–6% of the photoreceptors. However, the proportion of rods in the photoreceptor population varies with retinal location. This is shown for two retinas in Figure 6. The maps were obtained by combining the rod and cone data from Figure 5. Rods constitute between 1 and 14% of the photoreceptor population. The highest percentages of rods occur in

inferior retina, where the rod maximum is not paralleled by a cone maximum. In temporal retina the low rod percentage corresponds to the minimum in rod density. In all other parts of the retina the rod percentage is between 4 and 8%.

Presumed blue-sensitive cones. Figure 7 illustrates the distribution pattern of the more intensely stained, regularly arrayed cones (cf. Fig. 1C,D) at different locations. Their density decreases with the overall density of cones, from inferior retina (Fig. 7A) to superior retina (Fig. 7B). In

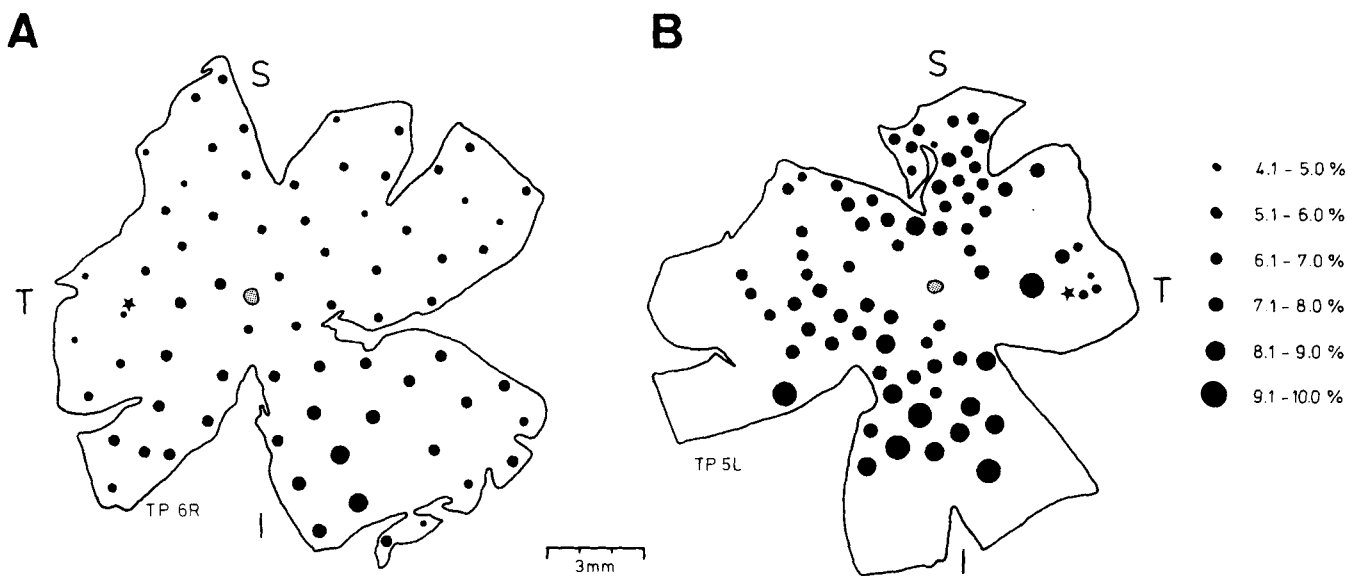


Fig. 8. Maps of the proportion of presumed blue-sensitive cones in the entire cone population for two retinas. Each dot represents a sample field and its size represents the local blue cone percentage. The two reti-

nae show slight differences in blue cone percentage, probably reflecting interindividual variability, but the trends are the same. Not corrected for shrinkage. The star marks the position of the central area.

the discussion it is argued that these are the blue-sensitive cones, and for the sake of simplicity this terminology is introduced here.

The blue-sensitive cones constitute between 4 and 10% of all cones depending on retinal location (Fig. 8). In the upper

retina the percentage of this subpopulation ranges between 4 and 6.5%, whereas the lower half contains upward of 7%. Maxima of about 10% are found in inferior and inferonasal midperiphery. Generally, the percentage of blue-sensitive cones increases with absolute cone density, except for a minimum in blue cone density and percentage in temporal retina near the central area.

A similar cone subpopulation was found by immunolabelling with an antibody against retinal S-antigen (Müller et al., '89); an example is shown in Figure 9. The immunopositive cones constitute between 4 and 10% of all cones, with the same topographical distribution as the more strongly stained cones in toluidine-blue-stained horizontal sections.

For technical reasons it was not possible to demonstrate the specific toluidine blue staining of immunopositive cones. Hence a statistical analysis was used to test the assumption that toluidine blue (TB) and the antibody against retinal S-antigen (SAP) both stain the same, presumed blue-sensitive, cone population; the mosaics of the two populations were compared quantitatively by a nearest-neighbour analysis (Wässle and Riemann, '78). For each subpopulation the distribution of nearest-neighbour distances was analysed in a region of low density (Fig. 10A,C) and in a field of higher density (Fig. 10B,D). All four histograms are better fitted by a Gaussian than a Poissonian distribution; i.e., their spacing is statistically regular. The precision of the arrangement can be expressed by the quotient of the mean over standard deviation of the distribution. The greater the value, the more regular the array. The values are 7.7 (TB) and 7.9 (SAP) for the low densities and 8.5 (TB) and 8.0 (SAP) for the high densities. In conclusion, both cone subpopulations are arrayed in a pattern with the same grade of regularity for corresponding densities. The pattern analysis is thus consistent with the assumption that both staining procedures label the same cone subpopulation.

Dark cones. The topographical distribution of the cone subpopulation with darkly stained, polygonal profiles

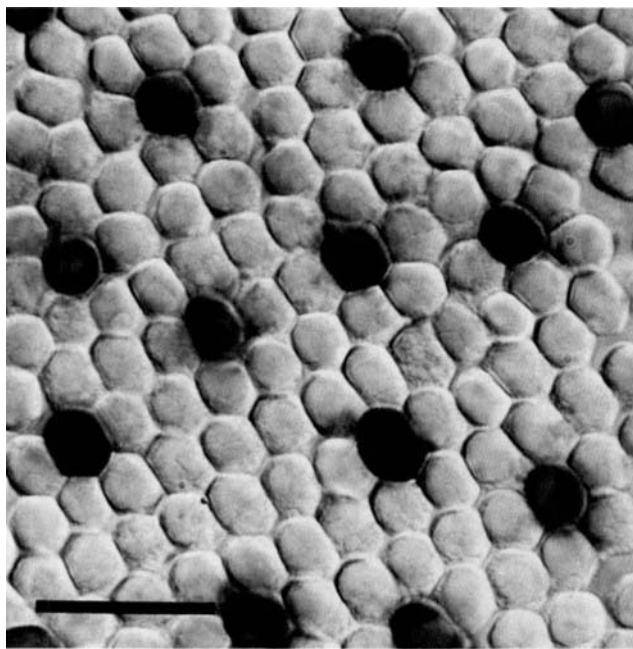


Fig. 9. Micrograph of a field of a whole-mounted retina stained with the S-antigen antibody, visualized with the peroxidase-antiperoxidase technique (Müller et al., '89). The focus is on the cone inner segments. The regular distribution of immunopositive presumed blue-sensitive cones is very prominent. Scale bar equals 20 μ m.

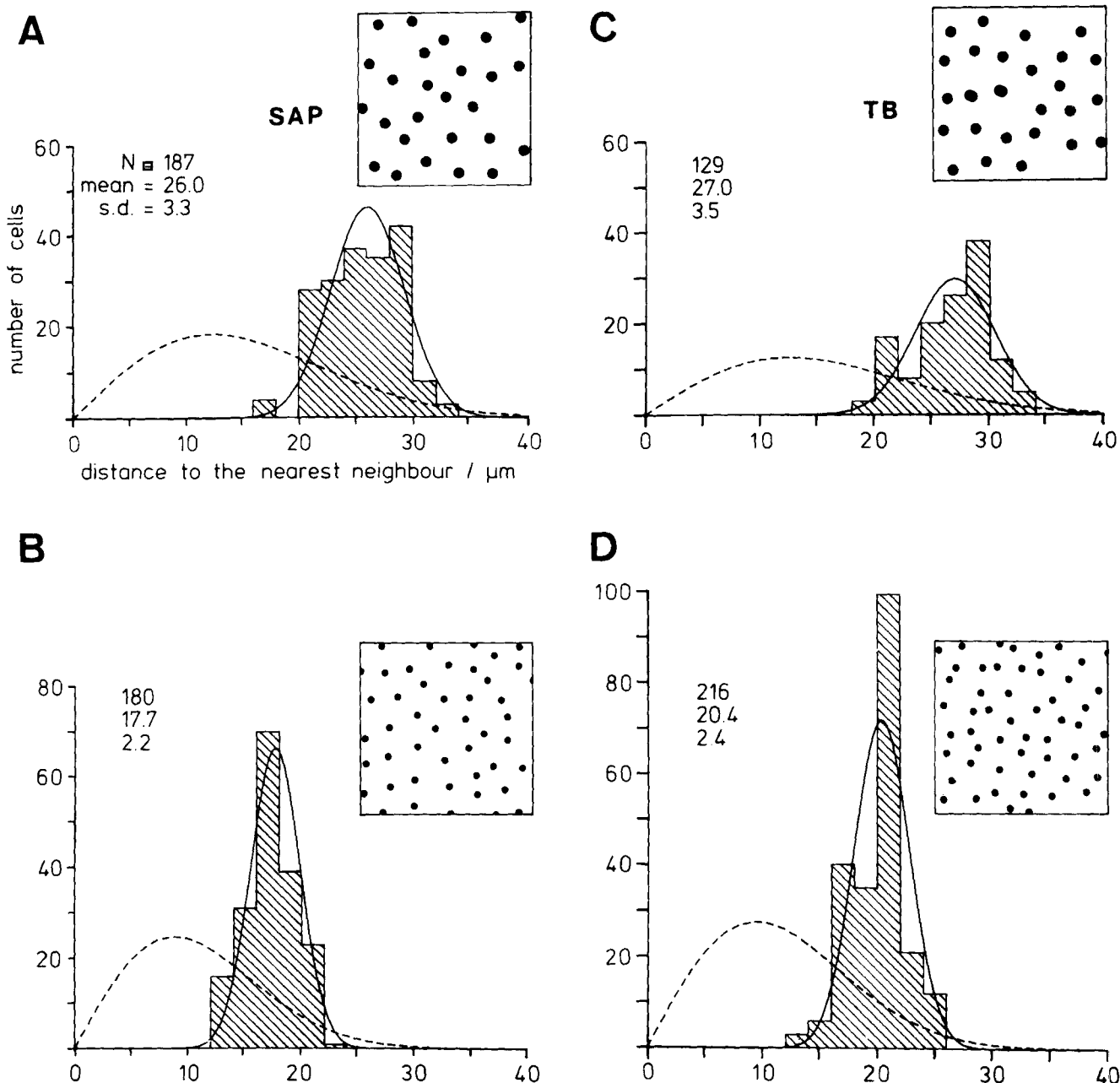


Fig. 10. Nearest-neighbour analyses of the presumed blue-sensitive cone population. The two staining methods toluidine blue (TB, right column) and S-antigen immunoreactivity (SAP, left column) are compared at two eccentricities. Histograms of nearest-neighbour distances are compared for a region of low density ($1,055/\text{mm}^2$ in A, $1,009/\text{mm}^2$ in C) and for a region of higher density ($2,034/\text{mm}^2$ in B, $1,760/\text{mm}^2$ in D).

The solid curves are Gaussian approximations of the nearest-neighbour distributions. The broken curves give the Poisson distribution of nearest neighbours for a random pattern of the same density (see Wässle and Riemann, '78). Insets: $250 \times 250 \mu\text{m}$ frames of the larger sample fields. The cone populations revealed by the two staining methods have the same grade of regularity. For details see text.

(cf. Fig. 1D,E) is rather irregular. The arrangement of these "dark cones" at three typical densities is shown in Figure 11. For one retina their relative density was assessed systematically and displayed as a percentage map, Figure 12. Over most of the retina the percentages range between 2 and 13%. In the periphery of superior and inferior retina and also near the papilla their percentage increases to 14–25%.

Occasionally they occur in small plaques with up to 100% dark cones (stippled areas). Dark cones were found in the retinae of all individuals, both those bred in captivity and those captured in the wild.

The dark cones correspond to one of the three cone types described by Foelix et al. ('87), and the present findings agree with their morphological description, except for the

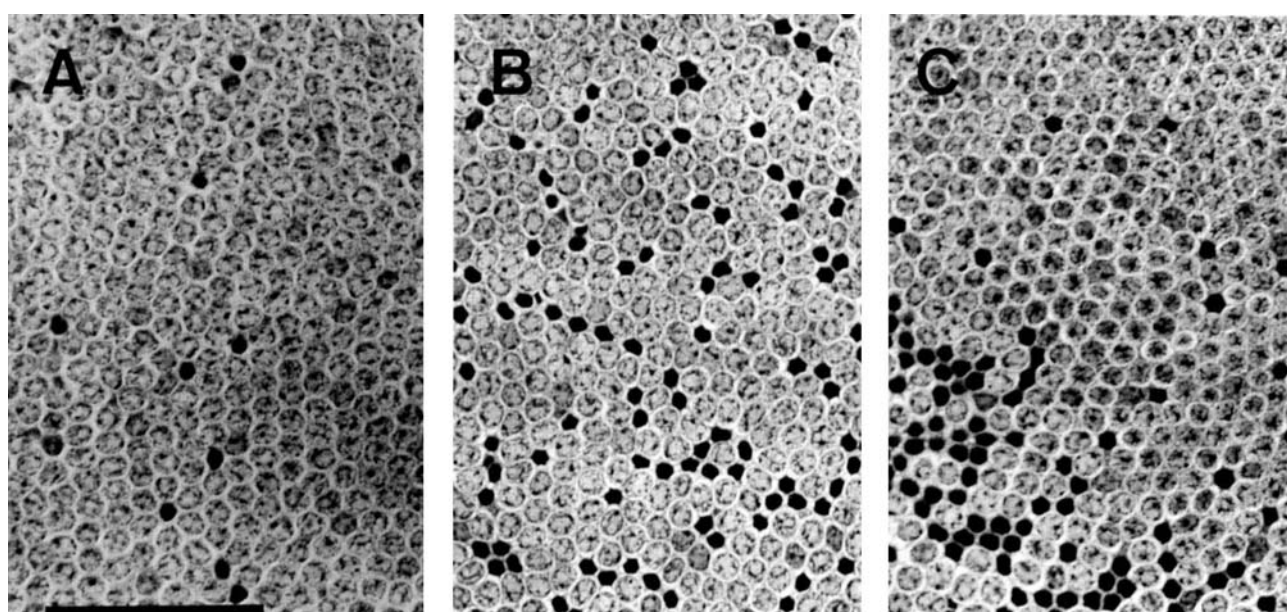


Fig. 11. Micrographs of toluidine-blue-stained horizontal sections through the outer nuclear layer, showing the density range and irregular distribution of "dark cones" in one retina. A: A very low proportion of dark cones (3%) is present in most parts of the retina. B: A higher pro-

portion (the field contains 25%) occurs in some regions. C: Boundary region of a small plaque of dark cones which extended to the left and contained only dark cones. Scale bar equals 50 μm for A-C.

occurrence of high-density patches. The dark cones differ from other cones in shape and their affinity for toluidine blue. The profiles of the inner segments and nuclei of these cones appear pyknotic and very dark, features characteristic of pathological phenomena, like degeneration, or an artefactual pyknosis induced by handling of the tissue (Cammert-meyer, '78). Their erratic distribution makes it unlikely that they contribute consistently to colour perception. All this

argues against the dark cones being a colour-specific cone type (see discussion of blue cones).

DISCUSSION

Photoreceptor topographies

The present study describes the topographical distribution of the different photoreceptor types in the tree shrew retina, each of which shows special distribution patterns. Of these types the rod population amounts to only 4–6% of all photoreceptors. In contrast, the cones represent some 95% with three subpopulations: 1) the presumed blue cones, which compose 4–10% of all cones, 2) the dark cones, which can constitute up to 25% of local cone densities, and 3) the majority (red) cones (as will be argued later).

The density of cones reaches a maximum ($32,000\text{--}36,000/\text{mm}^2$) in midperipheral nasal and inferior retina, and a minimum ($12,000/\text{mm}^2$) in superior periphery (Fig. 5). The density gradient is steepest toward inferior periphery. In all three retinae analyzed in detail the cone density maxima occurred at two distinct locations. The positions of the maxima were in nasal and inferior retina for two individuals and inferonasal and inferotemporal in the third. In no instances, however, did a maximum coincide with the position of the central area. Our results confirm Immel and Fisher's ('85) finding that the cone density in central retina is higher than in periphery and that the average cone density amounts to $25,000/\text{mm}^2$. In contrast to those results, however, we do not find particularly high cone densities in temporal retina.

The rod proportion of the entire photoreceptor population is between 1 and 14% depending on retinal location (Fig. 6). The highest rod density and percentage are located in inferior periphery ($3,500/\text{mm}^2$, 14%; Figs. 5, 6). This maximum is not congruent with the cone density maximum. From the inferior periphery to the central part of the retina

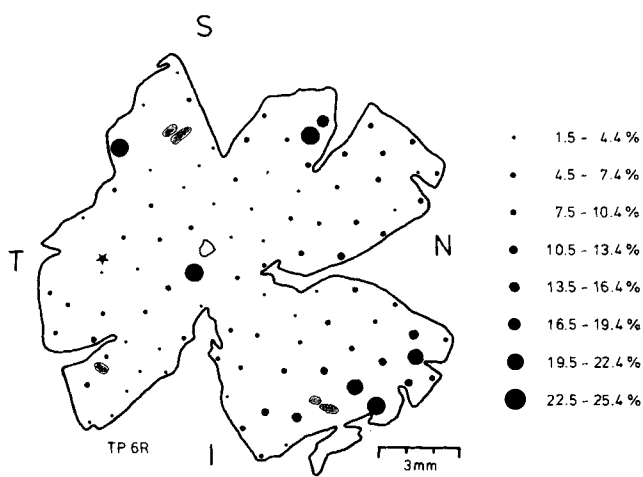


Fig. 12. Map of the proportion of dark cones in the total cone population of one retina. Each dot position and size represent a sample field and the local dark cone percentage. The outlined stippled areas represent small plaques of dark cones; the plain outlined area is the papilla. The dark cone proportion varies strongly over the retina; plaques are located in more peripheral regions. Not corrected for shrinkage. The star marks the position of the central area.

the rod percentages decrease to 4%. The lowest rod densities and percentages occur in superior and temporal periphery ($200/\text{mm}^2$, <2%; Figs. 5, 6). Here there is a discrepancy between the present study and the data of Immel and Fisher ('85). They report rod percentages from 1.7 to 7.8% with a maximal rod density and percentage in temporal periphery.

All retinae investigated here were carefully oriented according to external ocular marks and the blood-vessel pattern. A possible explanation for the inconsistency with Immel and Fisher's data might be a less-reliable criterion for orientation during processing of the retina. Also, their data, based on eight sample points across the retina, may have missed the photoreceptor extremes.

Presumed blue-sensitive cones

A regularly arrayed subpopulation of cones whose inner segments and nuclei stained more strongly than those of most other cones was observed in semithin, toluidine-blue-stained horizontal sections. They constitute between 4 and 10% of all cones depending on retinal location (Fig. 8). Maximal percentages occur in inferior nasal midperiphery in parallel with the maximum cone density. A density and percentage minimum is localized in temporal retina, where the total cone density has no minimum. For the following reasons, we consider this population to be the blue-sensitive cones.

In the primate retina (baboon) Marc and Sperling ('77) histochemically demonstrated the distribution of three types of cone by a light-stimulated reaction resulting in the reduction of nitroblue tetrazolium. They describe the blue-sensitive cones as a regularly distributed population having a low relative density (3–20%) changing with retinal location. Cone subpopulations with similar arrangements and distributions have been found to preferentially accumulate procion dyes in macaque and ground squirrel (De Monasterio et al., '81, '85; McCrane et al., '83; Ahnelt, '85) and to stain prominently with toluidine blue in human and ground squirrel (Long and Fisher, '83; Ahnelt et al., '87). Recently, a similar cone subpopulation was labelled by immunocytochemical methods in ground squirrel, human, grass monkey, rabbit, cow, pig, and tree shrew retina (Long and Aquirre, '87; Szél et al., '88; Müller et al., '89). It has been postulated that those cones represent the blue-sensitive cone population because of their distinct density and arrangement.

In the tree shrew retina, the cone subpopulation labelled with the S-antigen antibody (Müller et al., '89) has the same low relative density (4–10%) and the same regular distribution as the one stained prominently with toluidine blue (cf. Fig. 9). We conclude that both methods stain the same cones which, by comparison with the staining properties in other species, are regarded as blue-sensitive cones. This conclusion is supported by the microspectrophotometric measurements of Petry and Harosi ('87), who found two cone types in the tree shrew retina: a long-wavelength (557 nm), red-sensitive type and a short-wavelength (425 nm), blue-sensitive type. A third, middle-wavelength, green-sensitive type was not observed. This finding argued for dichromatic vision. Only eight of the 272 cones, or 3%, recorded by Petry and Harosi ('87) were of the blue-sensitive type; this value is in the same range as our labelled cone subpopulation. There is no support for the possibility that the S-antigen-immuno-reactive and the toluidine-blue-stained cones are different subpopulations with similar mosaics, one perhaps representing a green-sensitive cone type. The existence of only two functional cone types also argues against the dark cones being an additional colour-specific cone type.

The spectral sensitivity curve of the tree shrew retina, determined by electroretinogram recordings, shows a peak at about 552 nm, with an indication of a second peak at the blue end of the spectrum, suggesting increased blue sensitivity (Tigges et al., '67). This observation also corroborates the existence of a significant blue-sensitive cone population.

Functional considerations

The two functional cone types provide the diurnal tree shrew with reasonable daylight and colour vision, manifested in the electroretinogram (ERG) (Tigges et al., '67) and in behavioural performance (Tigges, '63; Shriner and Noback, '67). No rod component was detected in the ERG. The absolute dark-adapted threshold was high compared to duplex or rod retinae, and there was no evidence for a Purkinje shift, both of which suggested the absence of a scotopic system.

Here tree shrews can be compared with diurnal ground squirrels, which also have a cone-dominated retina and only a small rod population of 5–10% (Vaidya, '64; West and Dowling, '75; Jacobs et al., '80; Long and Fisher, '83). Detailed ERG studies of the ground squirrel revealed that under dark-adapted conditions, two-thirds of the tested animals had an ERG spectral sensitivity function resembling that predicted by the rhodopsin nomogram, and they showed a Purkinje shift. One third of the animals, however, showed no indication of a scotopic system in their ERG, although they all had a sparse rod population (Green and Dowling, '75; Jacobs et al., '76, '80). The authors concluded that a rod population of about 10% is the limit detectable by ERG recordings. So, it is not surprising that Tigges et al. ('67) did not find ERG evidence for scotopic vision in the tree shrew retina. Behavioural experiments also showed no indication of a rod contribution to the visual performance of tree shrews (Schäfer, '69). The sparse rod population of about 5% in the tree shrew retina is probably below the limit detectable by these methods.

If the rods play a role in visual information processing, this should be apparent in the ganglion cell receptive field properties under scotopic conditions. Such data are as yet not available.

In temporal retina the blood-vessel pattern and the ganglion cell distribution mark a central area in a rather peripheral position, within the binocular field representation. The cone distribution, on the other hand, shows no corresponding specialisation there. This is in contrast to other mammals, where regions of high ganglion cell density also have a high cone density (primate central retina: Polyak, '41; cat central area: Steinberg et al., '73; rabbit visual streak: Hughes, '71). However, the sparse rod population reaches its lowest densities in the central area, and this resembles the local rod density minimum in cat central area (Steinberg et al., '73).

Even with the lower cone density in the tree shrew's central area there is a convergence ratio of slightly more than one cone per ganglion cell (Müller and Peichl, unpublished observation) so that the resolution of the cones could be conserved to a large extent by the ganglion cells. Schäfer ('69) determined the visual acuity of the tree shrew behaviourally and found a resolution limit for gratings with a stripe width of 6.3' of arc (grating period 12.6' of arc, spatial frequency 4.8 cycles/deg). This stripe width corresponds to 7.4 μm on the retina, fitting reasonably with the cone spacing of 6 μm in the central area. Petry et al. ('84) reported acuities of 2.4 c/deg or less, corresponding to a stripe width of 14.7 μm or more on the retina and hence indicating some

convergence of cones. Differences in the experimental assays may account for the differing results, as discussed by Petry et al. ('84).

Maximal cone densities (cone spacing 3 μm) occur in inferior retina where the receptor mosaic and its potential for high resolution do not seem to be fully exploited, because ganglion cell density is lower and thus convergence greater.

The tupaia retina provides a striking example of a topographical arrangement wherein the photoreceptors and ganglion cells do not show corresponding maxima and minima. It has been argued that specialisations in the topography of retinal neurones reflect the necessities imposed onto an animal by its habitat ("terrain theory" of Hughes, '77; Collin and Pettigrew, '88a,b). The existence of a temporal, rather circular, central area in the tree shrew ganglion cell layer (DeBruyn, '83; Müller and Peichl, unpublished observations) accords with its arboreal lifestyle and is similar to the central area of cat and the fovea of primates. Climbing, grasping, and jumping require a high-acuity depth perception, which is best realized by a central area within the binocular field of view. (The laterally positioned eyes give the tree shrew a wide panoramic view, with a binocular field of 50–60°; Polyak, '57). The more streaklike distribution of the photoreceptors with maxima in inferior retina is, however, more reminiscent of the ground squirrel or rabbit arrangements, which are adapted to an open terrestrial habitat with a visible horizon (Hughes, '71, '77; Long and Fisher, '83). The photoreceptor concentration in inferior retina indicates an importance of the upper visual field in the behaviour of the tree shrew. However, to assess the impact of the photoreceptor distribution on the visual performance of the tree shrew it has to be elucidated how the photoreceptor array is reflected in the ganglion cells and in higher visual centres.

ACKNOWLEDGMENTS

We thank B.B. Boycott and J.F. Dann for their helpful comments on the manuscript, J. Schnitzer for advice on microglia histochemistry, and H. Wässle for support of the study. The excellent technical assistance of H. Ahmed is gratefully acknowledged. We also thank the two anonymous referees for their detailed, valuable comments. The study was supported by the Deutsche Forschungsgemeinschaft (SFB 45/C7).

LITERATURE CITED

- Ahnelt, P.K. (1985) Characterization of the color related receptor mosaic in the ground squirrel. *Vision Res.* 25:1557–1567.
- Ahnelt, P.K., H. Kolb, and R. Pfug (1987) Identification of a subtype of cone photoreceptor, likely to be the blue sensitive, in the human retina. *J. Comp. Neurol.* 255:18–34.
- Anderson, D.H., and G.H. Jacobs (1972) Color vision and visual sensitivity in the California ground squirrel (*Citellus beecheyi*). *Vision Res.* 12:1995–2004.
- Boycott, B.B., and J.M. Hopkins (1981) Microglia in the retina of monkey and other mammals; its distinction from other types of glia and horizontal cells. *Neuroscience* 6:679–688.
- Cammermeyer, J. (1978) Is the solitary dark neuron a manifestation of post-mortem trauma to the brain inadequately fixed by perfusion? *Histochemistry* 56:97–115.
- Castenholz, E. (1965) Über die Struktur der Netzhautmitte bei Primaten. *Z. Zellforsch.* 65:646–661.
- Collin, S.P., and J.D. Pettigrew (1988a) Retinal topography in reef teleosts I. Some species with well-developed areae but poorly-developed streaks. *Brain Behav. Evol.* 31:269–282.
- Collin, S.P., and J.D. Pettigrew (1988b) Retinal topography in reef teleosts II. Some species with prominent horizontal streaks and high-density areae. *Brain Behav. Evol.* 31:283–295.
- De Monasterio, F.M., E.P. McCrane, J.K. Newlander, and S.J. Schein (1985) Density profile of blue-sensitive cones along the horizontal meridian of macaque retina. *Invest. Ophthalmol. Vis. Sci.* 26:289–302.
- De Monasterio, F.M., S.J. Schein, and E.P. McCrane (1981) Staining of blue-sensitive cones of the macaque retina by a fluorescent dye. *Science* 213:1278–1281.
- DeBruyn, E.J. (1983) The Organization and Central Terminations of Retinal Ganglion Cells in the Tree Shrew (*Tupaia glis*). PhD Thesis, Nashville, Tennessee.
- Dieterich, C.E. (1969) Die Feinstruktur der Photorezeptoren des Spitzhörnchens (*Tupaia glis*). *Anat. Anz.* 125:305–312.
- Dräger, U.C. (1983) Coexistence of neurofilaments and vimentin in a neurone of adult mouse retina. *Nature* 303:169–172.
- Foelix, R.F., R. Kretz, and G. Rager (1987) Structure and postnatal development of photoreceptors and their synapses in the retina of the tree shrew (*Tupaia belangeri*). *Cell Tissue Res.* 247:287–297.
- Green, D.G., and J.E. Dowling (1975) Electrophysiological evidence for rod-like receptors in the gray squirrel, ground squirrel and prairie dog retinas. *J. Comp. Neurol.* 159:461–472.
- Hughes, A. (1971) Topographical relationships between the anatomy and physiology of the rabbit visual system. *Doc. Ophthalmol.* 30:33–159.
- Hughes, A. (1977) The topography of vision in mammals of contrasting life style: Comparative optics and retinal organisation. In F. Crescittelli (ed): *Handbook of Sensory Physiology*, Vol. VII/5: The Visual System of Vertebrates. Berlin: Springer Verlag, pp. 697–756.
- Immel, H., and S.K. Fisher (1985) Cone photoreceptor shedding in the tree shrew (*Tupaia belangeri*). *Cell Tissue Res.* 239:667–675.
- Jacobs, G.H., S.K. Fisher, D.H. Anderson, and M.S. Silverman (1976) Scotopic and photopic vision in the California ground squirrel: Physiological and anatomical evidence. *J. Comp. Neurol.* 165:209–228.
- Jacobs, G.H., B.H. Tootell, S.K. Fisher, and D.H. Anderson (1980) Rod photoreceptors and scotopic vision in ground squirrels. *J. Comp. Neurol.* 189:113–125.
- Korf, H.-W., M. Möller, I. Gery, J.S. Zigler, and D.C. Klein (1985) Immunocytochemical demonstration of retinal S-antigen in the pineal organ of four mammalian species. *Cell Tissue Res.* 239:81–85.
- Kühne, J.-H. (1983) Rod receptors in the retina of *Tupaia belangeri*. *Anat. Embryol. (Berl.)* 167:95–102.
- Long, K.O., and S.K. Fisher (1983) The distribution of photoreceptors and ganglion cells in the California ground squirrel, *Spermophilus beecheyi*. *J. Comp. Neurol.* 221:329–340.
- Long, K.O., and G.D. Aguirre (1987) Retinal S-antigen in mammalian cone photoreceptors. *Invest. Ophthalmol. Vis. Sci. (Suppl.)* 28:339 (Abstract).
- Marc, R.E., and H.G. Sperling (1977) Chromatic organization of primate cones. *Science* 196:454–456.
- McCrane, E.P., F.M. De Monasterio, S.J. Schein, and R.C. Caruso (1983) Non-fluorescent dye staining of primate blue cones. *Invest. Ophthalmol. Vis. Sci.* 24:1449–1456.
- Müller, B., L. Peichl, W.J. DeGrip, I. Gery, and H.W. Korf (1989) Opsin- and S-antigen-like immunoreactions in photoreceptors of the tree shrew retina. *Invest. Ophthalmol. Vis. Sci.* 30:530–535.
- Novikoff, A.B., and S. Goldfischer (1961) Nucleosidephosphatase activity in the Golgi apparatus and its usefulness for cytological studies. *Proc. Natl. Acad. Sci. USA* 47:802–810.
- Petry, H.M., R. Fox, and V.A. Casagrande (1984) Spatial contrast sensitivity of the tree shrew. *Vision Res.* 24:1037–1042.
- Petry, H.M., and F.I. Harosi (1987) Tree shrew visual pigments by microspectrophotometry. *Ann. NY Acad. Sci.* 494:250–252.
- Polley, E.H., and C. Walsh (1984) A technique for flat embedding and en face sectioning of the mammalian retina for autoradiography. *J. Neurosci. Methods* 12:57–64.
- Polyak, S.L. (1941) The Retina. Chicago: The University of Chicago Press.
- Polyak, S. (1957) The Vertebrate Visual System. Chicago: The University of Chicago Press.
- Rohen, J.W., and A. Castenholz (1967) Über die Zentralisation der Retina bei Primaten. *Folia Primatol. (Basel)* 5:92–147.
- Samorajski, T., J.M. Ordy, and J.R. Keefe (1966) Structural organisation of the retina in the tree shrew (*Tupaia glis*). *J. Cell Biol.* 28:489–504.
- Schäfer, D. (1969) Untersuchungen zur Sehphysiologie des Spitzhörnchens *Tupaia glis* (Diard 1820). *Z. Vergl. Physiol.* 63:204–226.
- Shriver, J.E., and C.R. Noback (1967) Color vision in the tree shrew (*Tupaia glis*). *Folia Primatol. (Basel)* 6:161–169.
- Steinberg, R.H., M. Reid, and P.L. Lacy (1973) The distribution of rods and cones in the retina of the cat (*Felis domesticus*). *J. Comp. Neurol.* 148:229–248.

- Szél, Á., T. Diamantstein, and P. Röhlich (1988) Identification of the blue-sensitive cones in the mammalian retina by anti-visual pigment antibody. *J. Comp. Neurol.* 273:593-602.
- Terubayashi, H., Y. Murabe, H. Fujisawa, M. Itoi, and Y. Ibata (1984) Enzymehistochemical identification of microglial cells in the rat retina: Light and electron microscopic studies. *Exp. Eye Res.* 39:595-603.
- Tigges, J. (1963) Untersuchungen über den Farbensinn von *Tupaia glis* (Diderd 1820). *Z. Morphol. Anthropol.* 53:109-123.
- Tigges, J., B.A. Brooks, and M.R. Klee (1967) ERG recordings of primate pure cone retina (*Tupaia glis*). *Vision Res.* 7:553-563.
- Vaidya, P.G. (1964) The retina and the optic nerve of the ground squirrel *Citellus tridecemlineatus*. *J. Comp. Neurol.* 122:347-353.
- Wässle, H., W.R. Levick, and B.G. Cleland (1975) The distribution of the alpha type of ganglion cells in the cat's retina. *J. Comp. Neurol.* 159:419-438.
- Wässle, H., and H.J. Riemann (1978) The mosaic of nerve cells in the mammalian retina. *Proc. R. Soc. Lond. [Biol.]* 200:441-461.
- West, R.G., and J.E. Dowling (1975) Anatomical evidence for cone and rod-like receptors in the gray squirrel, ground squirrel, and prairie dog retinas. *J. Comp. Neurol.* 159:439-460.